OPEN ACCESS
IOP Publishing
Nanotechnology

Nanotechnology **29** (2018) 285601 (8pp)
https://doi.org/10.1088/1361-6528/aabec0

n-type doping and morphology of GaAs nanowires in Aerotaxy

Wondwosen Metaferia[1,2,4], Sudhakar Sivakumar[1,2], Axel R Persson[1,3], Irene Geijselaers[1,2], L Reine Wallenberg[1,3], Knut Deppert[1,2], Lars Samuelson[1,2] and Martin H Magnusson[1,2,4]

[1] NanoLund, Lund University, Box 118, SE-22100, Lund, Sweden
[2] Solid State Physics, Lund University, Box 118, SE-22100, Lund, Sweden
[3] nCHREM/Center for Analysis and Synthesis, Lund University, Box 124, SE-22100, Lund, Sweden

E-mail: wondwosen.metaferia@nrel.gov, wtm@kth.se and martin.magnusson@ftf.lth.se

Received 15 February 2018, revised 25 March 2018
Accepted for publication 17 April 2018
Published 10 May 2018

Abstract

Controlled doping in semiconductor nanowires modifies their electrical and optical properties, which are important for high efficiency optoelectronic devices. We have grown *n*-type (Sn) doped GaAs nanowires in Aerotaxy, a new continuous gas phase mass production technique. The morphology of Sn doped nanowires is found to be a strong function of dopant, tetraethyltin to trimethylgallium flow ratio, Au–Ga–Sn alloying, and nanowire growth temperatures. High temperature and high flow ratios result in low morphological quality nanowires and in parasitic growth on the wire base and surface. Alloying and growth temperatures of 400 °C and 530 °C, respectively, resulted in good morphological quality nanowires for a flow ratio of TESn to TMGa up to 2.25×10^{-3}. The wires are pure zinc-blende for all investigated growth conditions, whereas nanowires grown by metal-organic vapor phase epitaxy with the same growth conditions are usually mainly Wurtzite. The growth rate of the doped wires is found to be dependent more on the TESn flow fraction than on alloying and nanowire growth temperatures. Our photoluminescence measurements, supported by four-point probe resistivity measurements, reveal that the carrier concentration in the doped wires varies only slightly (1–3) $\times 10^{19}$ cm^{-3} with TESn flow fraction and both alloying and growth temperatures, indicating that good morphological quality wires with high carrier density can be grown with low TESn flow. Carrier concentrations lower than 10^{19} cm^{-3} can be grown by further reducing the flow fraction of TESn, which may give better morphology wires.

Supplementary material for this article is available online

Keywords: GaAs nanowires, *n*-type doping, Aerotaxy

(Some figures may appear in colour only in the online journal)

1. Introduction

Semiconductor nanowires are promising building blocks for optoelectronic devices such as light-emitting diodes [1], sensors [2], field effect transistors [3], and solar cells [4]. The advantage of nanowires lies mainly in the freedom to grow and combine otherwise incompatible materials, allowing advanced bandgap engineering and not least integration on silicon. Of particular interest to the work presented here, solar cells employing semiconductor nanowires have the potential for low cost and high energy conversion efficiency [5]. This is due to the nanowires' enhanced light absorption per atom as compared to thin films [6].

Most commonly, epitaxy is the method to produce III–V nanowires by different techniques, such as metal-organic

[4] Authors to whom any correspondence should be addressed.

vapor phase epitaxy (MOVPE) [7, 8], molecular beam epitaxy [9, 10] and chemical beam epitaxy [11, 12]. Although these techniques have proved to be effective in controlling crystal structure, dimension, material composition, and overall optoelectronic properties, they are slow and batch-based. Low growth rate, small substrate size and limited availability of native III–V substrates, and the high cost for materials fabrication, limit the commercial development of epitaxial growth of nanowires. For nanowires to be used in commercial applications, the current batch-based processes for nanowire production should be complemented by mass production techniques. Aerotaxy is demonstrated to be an efficient and continuous process to mass-produce nanowires with good crystallinity, dimension, and control of material composition [13, 14]. In Aerotaxy, an aerosol of size-selected Au catalyst nanoparticles (NPs) in N_2 is mixed with, for the intended growth, suitable combination of MOVPE precursors (trimethylgallium, TMGa; arsine, AsH_3; diethylzinc, DEZn; and tetraethyltin, TESn) in a flow-through reactor at atmospheric pressure, whereby nanowires are produced continuously at high density and high growth rate of about 1 μm s^{-1}, a growth rate 2–3 orders of magnitude higher than substrate based MOVPE growth. However, in order to use Aerotaxy for the fabrication of nanowire-based optoelectronic devices, controlled doping of III–V nanowires is very important. Only with controlled doping can the mobility, minority carrier diffusion length/time and conductivity be tuned. Controlled doping of nanowires is challenging due to process incompatibility, i.e., optimized growth parameters for undoped wire growth often do not favor the incorporation of dopant atoms, and different growth parameters are used for *n*- and *p*-type dopants. Compared to doping of III–V thin films, the presence of the Au catalyst particle further complicates doping of nanowires. The growth mechanisms and hence principles of dopant incorporation differ to a large extent among different growth techniques because of the variations in surface chemistry, precursor decomposition, and adatom migration [15]. Being a radically new and recently developed nanowire growth technique, there is still a lack of understanding and experimental work on both *n*- and *p*-type doping of semiconductor nanowires in Aerotaxy. Although *p*-type doping of GaAs nanowires in Aerotaxy by using DEZn as a dopant source [16], and a high quality *p*–*n* junction in Aerotaxy grown GaAs nanowires by Zn and Sn doping [17], has been demonstrated, the effect of growth parameters on wire quality and carrier concentration was not thoroughly discussed and *n*-type doping of GaAs wires was not investigated in detail. In this work, we demonstrate successful *n*-type doping of GaAs nanowires by using TESn as a dopant source and systematically investigate the effect of growth parameters on the morphology of the wires.

In this study we have investigated the dependence of the incorporation of active Sn dopant and nanowire morphology on the input TESn flux (expressed as the ratio of TESn to TMGa) as well as on the Ga–Au–Sn alloying and nanowire growth temperatures. As will be explained in the next section in detail, the Aerotaxy growth system employed here has three temperature zones. In the first zone, the group III precursor, TMGa, is added to the aerosol of Au NPs and preheated to form a Ga–Au alloy. For *n*-doping, TESn is also added at this stage and the effect of alloying temperature (T_a) was investigated. The group V precursor, AsH_3, is added in the second temperature zone, where growth of the nanowires takes place at the growth temperature (T_g). We varied T_g and investigated the effect on the nanowire morphological and optoelectronic qualities, while the third zone temperature (needed to keep the T_g profile stable) was fixed at 130 °C for all experiments. These temperatures are based on previous experiments in this growth reactor. The morphology of the nanowires was studied by scanning electron microscopy (SEM), and transmission electron microscopy (TEM) was used to examine their crystal phase and crystalline quality. Low temperature (7 K) photoluminescence (PL) and electrical four-point probe measurements were used to investigate the optical and electrical properties of the wires, from which carrier concentrations were estimated. We performed both four-point probe measurements and low temperature PL measurements on some of the samples; the carrier concentrations obtained from four-point probe analysis were found to be comparable to those obtained from low temperature PL measurements. Low temperature PL was therefore used to estimate the carrier concentrations in all the remaining samples. By using x-ray energy dispersive spectroscopy (XEDS) in TEM, we studied the composition of the seed NP for different growth conditions.

2. Experimental

Size-selected Au NPs were generated by an aerosol system as described by Magnusson *et al* [18] where the aerosol is formed by evaporating metallic Au at ∼1800 °C in a tube furnace. The vapor is carried out from the furnace by a continuous flow of N_2 at 1.5 l min^{-1}, and upon cooling, NP aggregates of various shapes and sizes are formed. The particles are reshaped into compact spheres in a sintering tube furnace at 550 °C, and a radial differential mobility analyzer (DMA) [19] is then used for size selection, typically set to 80 nm in diameter. The size-selected Au aerosol is then transported to the flow-through Aerotaxy reactor, before which the group III precursor TMGa and the TESn for doping are added.

In the reactor, the aerosol is preheated to an alloying temperature T_a to form a liquid Ga–Au alloy [20]. The group V precursor (AsH_3) is added to the aerosol in the second stage, at the temperature T_g, while the third zone temperature is fixed at 130 °C. Downstream the Aerotaxy reactor, the nanowire product can be collected on any substrate in an electrostatic precipitator with a collection voltage of 10 kV, equipped with a pump/purge system and placed inside a glove box. Figure 1 shows a simplified schematic of the Aerotaxy growth reactor used in this work.

The alloying and growth temperatures, as well as the partial pressure ratio of TESn/TMGa were varied to study the effect of these growth parameters on the resulting GaAs:Sn nanowires in terms of energy bandgap, morphological,

Alloying	Growth	Cool-down
430 °C	550 °C	130 °C
430 °C	530 °C	130 °C
400 °C	530 °C	130 °C

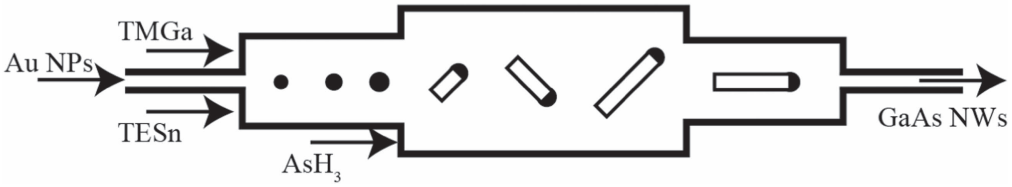

Figure 1. Simplified schematic of the Aerotaxy system used in this work (not to scale). Size-selected Au particles, TMGa, and TESn in N_2 carrier gas are introduced at the first stage of the reactor (alloying stage) at a temperature of T_a and AsH_3 is introduced in the second stage from the side. Nanowire growth starts at this stage at a growth temperature of T_g. The nanowires are collected on a silicon substrate in an electrostatic precipitator. The three temperature combinations used in this work are shown in the figure.

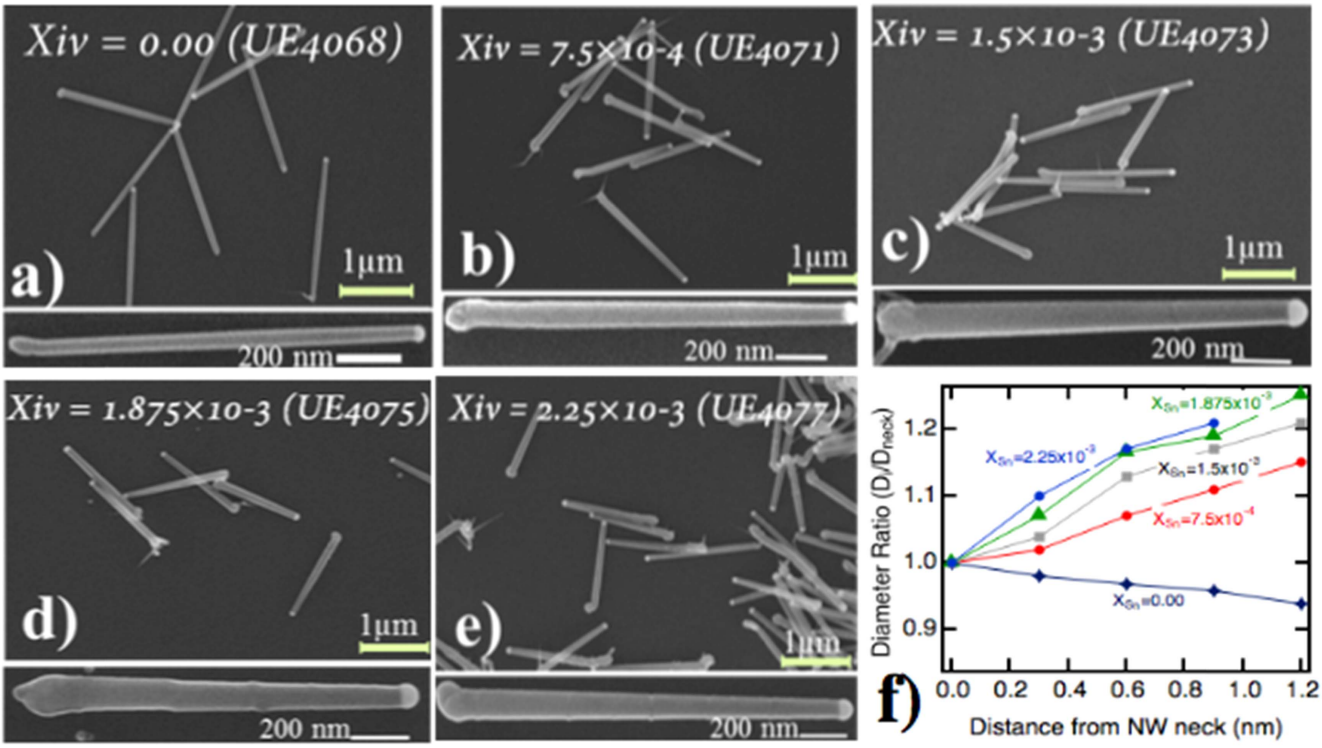

Figure 2. SEM images of Sn doped GaAs nanowires grown with (a) $X_{Sn} = 0.00$, (b) $X_{Sn} = 7.5 \times 10^{-4}$, (c) $X_{Sn} = 1.5 \times 10^{-3}$, (d) $X_{Sn} = 1.875 \times 10^{-3}$ and (e) $X_{Sn} = 2.25 \times 10^{-3}$. The alloying and growth temperatures in all cases are 400 °C and 530 °C, respectively. In each case, the lower panel is a SEM image of representative single nanowire. (f) Plot of relative diameter (measure of tapering) of the nanowire at different distance from the nanowire neck.

optoelectronic and structural qualities. By varying T_a and T_g as in figure 1 and X_{Sn} (TESn/TMGa) from 0 to 2.25×10^{-3}, a total 15 growth experiments were done and the resulting nanowires were collected during 5 min on Si substrates. In all experiment, the molar fractions of TMGa and AsH_3 were 2.8×10^{-4} and 2.4×10^{-4} respectively, i.e., a V/III of 0.82.

SEM was used to study the morphology of the nanowires, and also for measuring their length distribution. The structural quality of the wires was investigated by TEM in a Jeol 3000F microscope operating at 300 kV. For compositional analysis, XEDS (in the TEM) and low temperature PL were used. For PL measurements, the samples were excited with a frequency doubled solid state laser emitting at 532 nm, focused on the sample with a resulting excitation power density of approximately 200 W cm^{-2}. The ensemble PL signal originates from tens to hundreds of nanowires, depending on random local variations on the sample, see figure 2. The samples were kept in a liquid helium flow cryostat at 7 K. For the electrical four-point probe measurements [21], suitable devices were fabricated from single nanowires. The fabrication process begins with transferring the nanowires on to a silicon substrate covered with a gate oxide (100 nm SiO_2 and 10 nm HfO_2). Extensive SEM maps were constructed in order to select suitable wires for contacting. The substrate was then spin coated with a PMMA 950 A6 lift-off layer. Metal contacts were then defined by electron

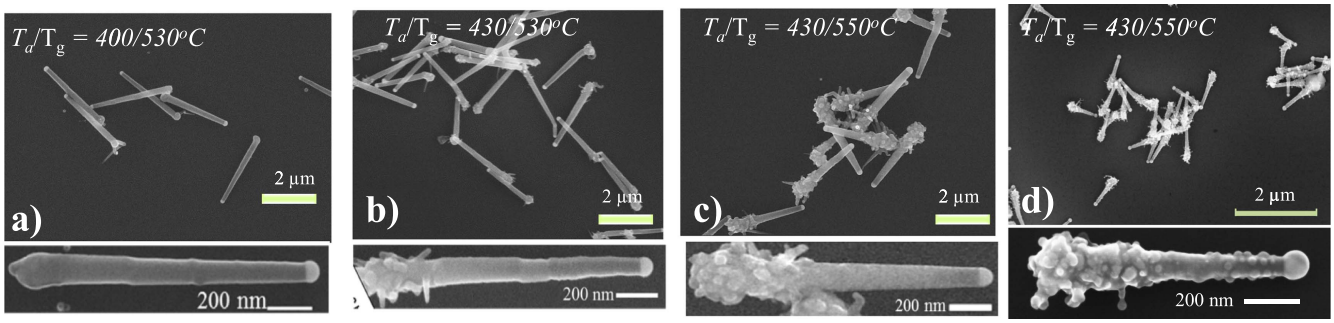

Figure 3. SEM images of GaAs nanowires grown at different alloying and the growth temperature of (a) $T_a/T_g = 400/530$ °C, (b) $T_a/T_g = 430/530$ °C, and (c) $T_a/T_g = 430/550$ °C and with same IV/III ($X_{Sn} = 1.875 \times 10^{-3}$) and (d) $T_a/T_g = 430/550$ °C as in (c) but with $X_{Sn} = 5 \times 10^{-3}$. See supplementary information for complete comparison of the effect of T_a/T_g at different X_{Sn}.

beam lithography and depositing 20 nm Pd, 80 nm Ge, followed by 100 nm Au. In order to improve ohmic behavior, the contacts were then annealed at 280 °C for 30 s.

3. Results and discussions

Figures 2(a)–(e) are SEM images of Sn doped GaAs nanowires grown at different TESn/TMGa ratios (X_{Sn}) at alloying and growth temperatures of 400 °C and 530 °C, respectively. The morphology of the wires changes as X_{Sn} increases. Undoped ($X_{Sn} = 0.00$) GaAs nanowires, figure 2(a), are mainly straight with no apparent tapering and with smooth surface morphology (in this paper, we use the term 'undoped' for simplicity, although the more correct term should be 'not intentionally doped'). The wires become more tapered and the surface becomes rougher as X_{Sn} increases. Figure 2(f) shows the plot of relative diameter (i.e., the ratio of the wire diameter depending on the distance to the wire diameter at the neck region). The relative diameter is the average from 10 NWs in each case. The diameter variation from wire to wire is less than 15% regardless of the distance from the NWs' neck where it is measured. The size of Au seed NPs is 80 ± 10 nm eventhough our set value for our DMA is 80 nm indicating the NW diameter distribution is not affected by the Sn doping. As can be seen from the plot, the addition of more TESn tends to make the wires tapered. In fact the opposite happened for the undoped wire where the diameter gradually shrinks towards the end, this indicates that adatom migration to the growth site in Aerotaxy is predominantly from direct impingement at the catalyst particle. In all cases of the doped wires (can also be seen in undoped wires rearly), the base of the wires is wider and polycrystalline; this is a general feature of Aerotaxy, attributed to random growth initiation defects before the wire finds a fast growing ⟨111⟩ *B* direction [13].

The morphology of the wires grown at different alloying and growth temperatures but same X_{Sn} was studied and representative SEM images are presented in figures 3(a)–(c). Nanowires grown at $T_a = 400$ °C and $T_g = 530$ °C are shown to have good morphology throughout the investigated range of X_{Sn}. On the other hand, nanowires grown at $T_a = 430$ °C and $T_g = 530$ °C are shown to be rougher, and parasitic growth at the base of the nanowires is observed for

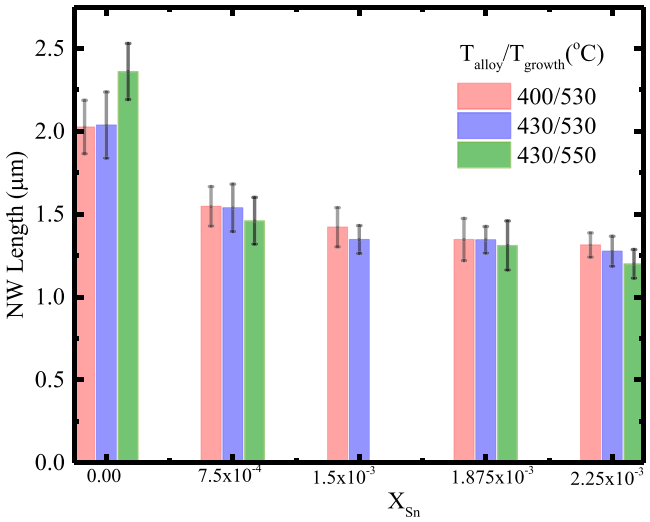

Figure 4. The average length of GaAs:Sn nanowires grown at different alloying and growth temperatures and TESn/TMGa ratio (X_{Sn}). The error bars represent the length standard deviations based on measurement of 20 wires.

the wires grown with the highest TESn flows. This tendency of parasitic growth and forming outgrowths on the wires is more aggressive for nanowires grown at alloying temperature of 430 °C and growth temperature of 550 °C. As can be seen from the SEM images (also in supplementary information, available online at stacks.iop.org/NANO/29/285601/mmedia), nanowire morphology is a factor of both alloying and growth temperatures and of X_{Sn}, i.e., higher alloying and growth temperatures and higher flows of TESn precursor result in wires with lower morphological quality.

The nanowire length was measured from SEM images and the average length of 20 nanowires from each sample plotted against X_{Sn} and alloying/growth temperatures see figure 4.

Considering the average length of the undoped wires, the growth rate increases with T_g, but appears unaffected by T_a. This is expected, since the growth rate determining step is the incorporation of adatoms in the crystal lattice which is not formed at the alloying stage in the absence of the AsH_3. The addition of Sn (TESn) precursor significantly suppresses the growth rate of the wires, reduced to almost half the rate of the undoped wires. As mentioned before, the wires become

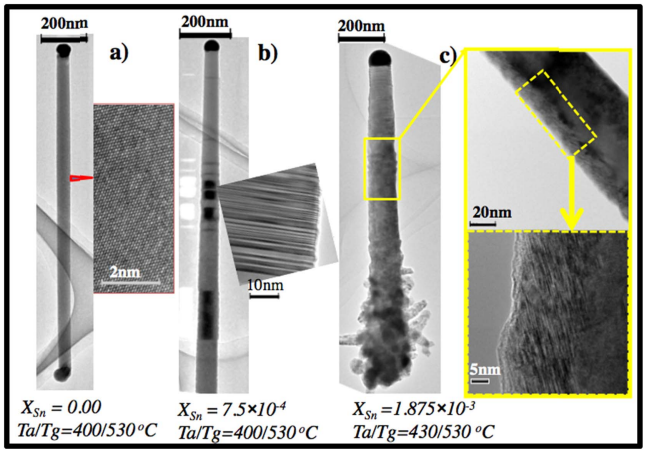

Figure 5. Transmission electron microscope images of GaAs nanowires grown (a) undoped (b) doped with $X_{Sn} = 7.5 \times 10^{-4}$ grown at 400 °C and 530 °C alloying and growth temperatures, respectively, and (c), doped with $X_{Sn} = 1.875 \times 10^{-3}$ grown at 430/550 °C alloying/growth temperatures. The inset in (a) shows the ZB crystal structure of the nanowire and the inset in (b) shows the twin defects caused by the Sn doping. Part of the nanowires in (c) indicated by a yellow rectangle was further analyzed by high resolution TEM showing signs of radial growth.

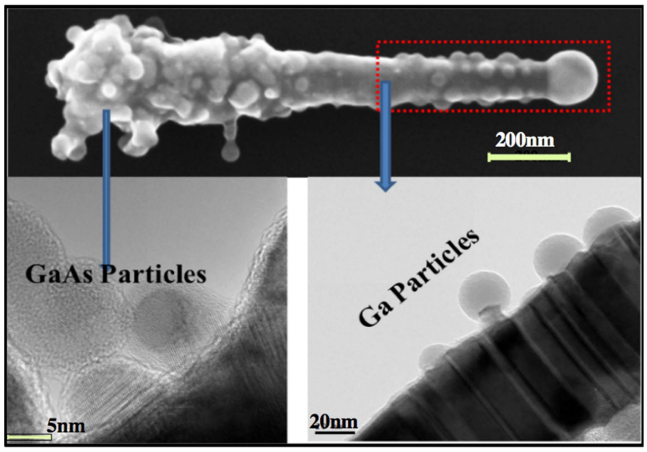

Figure 6. High resolution TEM studies of the parasitic nanoparticles and branches of a GaAs nanowire grown at Ta/Tg = 430/450 °C and $X_{Sn} = 5 \times 10^{-3}$. EDXS studies reveal that the particles/branches at the base of the nanowire are GaAs in composition whereas those in the upper half of the nanowire are Ga particles.

Table 1. XEDS elemental quantification of Sn in the catalyst nanoparticle; the measurements were done by averaging from five nanowires in each sample.

Sn (at%)			
	T_a/T_g(°C)		
X_{Sn}	400/530	430/530	430/550
7.5×10^{-4}	—	9	—
1.5×10^{-3}	6	10	19.0
1.875×10^{-3}	—	13	—
2.25×10^{-3}	11	14	20

tapered under TESn flow. This is attributed to a reduction of the mean diffusion length of rate limiting growth species for increased TESn flux. The increased growth temperature from 530 °C to 550 °C could enhance the decomposition of TESn resulting in increased Sn adatoms at the growth site which could further reduce the mean diffusion length and hence reduction of the growth rate at that growth temperature (figure 4). As the axial growth rate is reduced by the adatom mean diffusion length, the radial growth rate increases, resulting in tapering. On the nanowires grown at the higher T_g and flow of TESn, lateral growth leads to parasitic elongated particles, and in some cases we observe wires (hereafter called branches) of length reaching hundreds of nanometers. The adatom migration to the growth site in Aerotaxy can occur either by diffusion along the nanowire sidewall or from direct impingement at the catalyst particle. The reduced diffusion length/mobility of the Ga atoms on the surface of the nanowires can result in a higher lateral growth which results in tapering and even to the nucleation of Ga NPs. These NPs can act as catalysts for the growth of parasitic GaAs outgrowths or branches on the surface of the nanowires. Electron diffraction pattern studies in TEM on Sn doped GaAs nanowires reveal exclusively zinc-blende structure with twin defects whose density increases with X_{Sn} (figure 5).

High resolution TEM studies on the parasitic NPs and branches revealed their crystalline nature and confirm the above-suggested hypothesis on their formation (figure 6).

It can be seen that there is a clear interface between the wire and these particles, confirming that the particles/branches are formed at a later stage of the nanowire growth. TEM-XEDS studies of these particles/branches revealed that the particles/branches at the base of the nanowire are GaAs in composition and those in the upper part of the nanowire is Ga. This indicates that the parasitic GaAs particles/branches formation is a result of Ga catalyzed GaAs growth similar to droplet epitaxy [22]. Presumably, the Ga particles on the upper part of the wire have not had time to form GaAs, and/or have been deposited at a low temperature as the wire was leaving the growth zone.

To gain an insight into the Sn doping mechanism of GaAs nanowires in Aerotaxy, XEDS in TEM studies on the Au NP was done on selected samples grown at different alloying and growth temperatures. The Sn atomic % increases with X_{Sn} and the trend is stronger at higher alloying and growth temperatures. This indicates that the driving force for dopant incorporation in the wires is the Sn concentration in the catalyst particle (table 1). The fact that this concentration increased with alloying, growth temperature, as well as TESn/TMGa ratio, and that lower alloying and growth temperatures at lower TESn partial pressure resulted in better wire morphology, indicates that a possible cause of morphology change is a phase change in the Au–Ga–Sn alloy particle. The phase diagram for Au–Sn–Ga(–As) is not known well enough for more quantitative conclusions.

To investigate the optical properties of Sn doped GaAs nanowires, as-grown wire ensembles collected on Si substrates were cooled down to 7 K in a liquid helium cryostat, and μ-PL spectra were collected from different spots on the

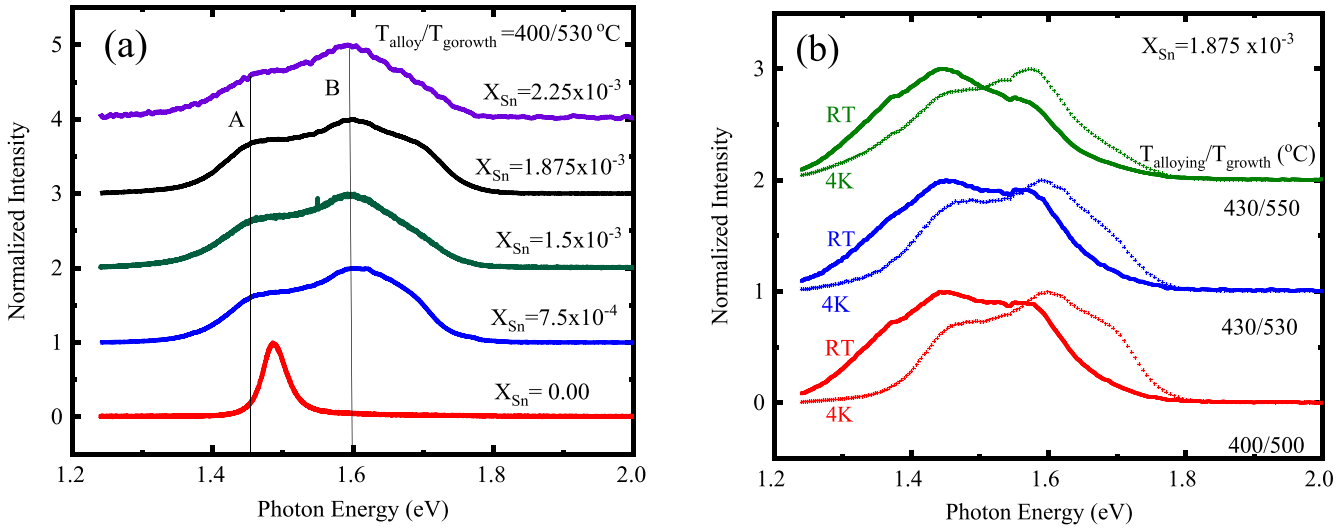

Figure 7. (a) 7 K PL spectra of Sn doped GaAs nanowires grown at different X_{Sn} (0.00–2.25 × 10^{-3}) and alloying and growth temperatures of 400/530 °C, and (b) room temperature and 7 K PL spectra of Sn doped GaAs nanowires grown at different alloying and growth temperatures but same X_{Sn} of 2.25 × 10^{-3} (b).

samples. The PL spectra in figure 7(a) come from GaAs nanowire samples grown at T_a = 400 °C and T_g = 530 °C, respectively and with varying X_{Sn} (0.00–2.25 × 10^{-3}). Figure 7(b) shows room temperature (RT) and low temperature (7 K) PL spectra from Sn doped GaAs nanowires grown at different T_a and T_g but with the same X_{Sn}. All spectra are normalized and plotted with an offset in intensity, for the purpose of clarity. In all of the spectra in figure 7(a), two major peaks A and B could be observed. Peak A at 1.46 eV is regarded in literature as a band-acceptor transition due to carbon impurities [23]. As in the case for MOVPE [24, 25] carbon is a dominant acceptor impurity also in GaAs nanowires grown by Aerotaxy, as it comes from the dissociation of TMGa and TESn used as a precursor for Ga in both cases. Studies of thin film epitaxy have shown that the (111)B surface orientation exhibits the highest degree of carbon incorporation [24]. Aerotaxy GaAs nanowires are shown to be exclusively [111]B-oriented [13], hence the high carbon impurities. High V/III ratio has been shown to reduce carbon impurities in MOVPE grown III–V layers by suppressing the adsorption of CH_3 radicals (the dissociation product of TMGa) [24]. AsH_3 pyrolysis produces atomic hydrogen that forms volatile methane (CH_4) and leaves the reactor as exhaust. This removes the carbon containing (CH_3) radical from the growth site and reduces the carbon impurity in the epi-layer. PL studies from undoped GaAs (figure 7(a)) nanowires shows no carbon peak as in the doped wires. This means the V/III ratio is optimal, i.e. the AsH_3 flow is enough to remove the carbon containing (CH_3) produced from the dissociation of TMGa. However, the dissociation product of TESn is still the source of carbon in the nanowires and additional AsH_3 required to remove the carbon contaminant. Thus, nanowires with better purity can be grown at higher AsH_3 flow (higher V/III ratio) or from a different *n*-type dopant precursor such as hydrogen sulfide.

The second, peak B at 1.60 eV corresponds to highly Burstein–Moss shifted band-to-band emission in heavily *n*-doped GaAs. The heavy doping could increase the average recombination energy and broadens the spectra by shifting the Fermi level in to the conduction band. As can be seen from figures 7(a) and (b), the low temperature and RT PL spectra from the doped GaAs are similar both in terms of peak energies and line shape, regardless of alloying and growth temperatures as well as the TESn/TMGa ratio, X_{Sn}. The carrier concentration of the doped GaAs nanowires is extracted from the low temperature PL by using a Fermi-tail fitting method by taking in to consideration the changes in effective carrier mass and bandgap renormalization [26]. As this approach applies to degenerately doped samples and works most accurately with high carrier concentrations (~4 × 10^{18} cm^{-3} and more), in order to estimate the carrier concentrations from the energy half-width of the band-to-band emission line in the PL spectra for the undoped samples, we used the empirical relation by De-Sheng *et al* [27]

$$\Delta E(n) = 3.84{*}n^{2/3}(\text{eV}), \quad (1)$$

where ΔE is measured in eV and n is given in cm^{-3}. The carrier concentrations estimated from 7 K PL by Fermi-tail fitting method and equation (1) for doped and undoped GaAs nanowires correspondingly are given in figure 8(a).

The four-point probe measurements were carried out by passing a current through probes 1 and 4 while measuring the voltage in probes 2 and 3 (figure 8(b) inset). The calculated resistivity is compared with the resistivity versus carrier concentration data from Sze and Irvin [28], the extracted carrier concentration for various IV/III ratios is given in figure 8(b). We note that a quantitative comparison of carrier concentrations in figures 8(a) and (b) shows a dispersion of carrier concentration for each X_{Sn} in figure 8(b). The data extracted using Fermi-tail fitting is seemingly in the high end for different X_{Sn}. This phenomenon is attributed to the fact that in PL measurements, a cluster of nanowires rather than a single NW radiates the detected signal, which is not the case in four-point probe measurements. The carrier concentration

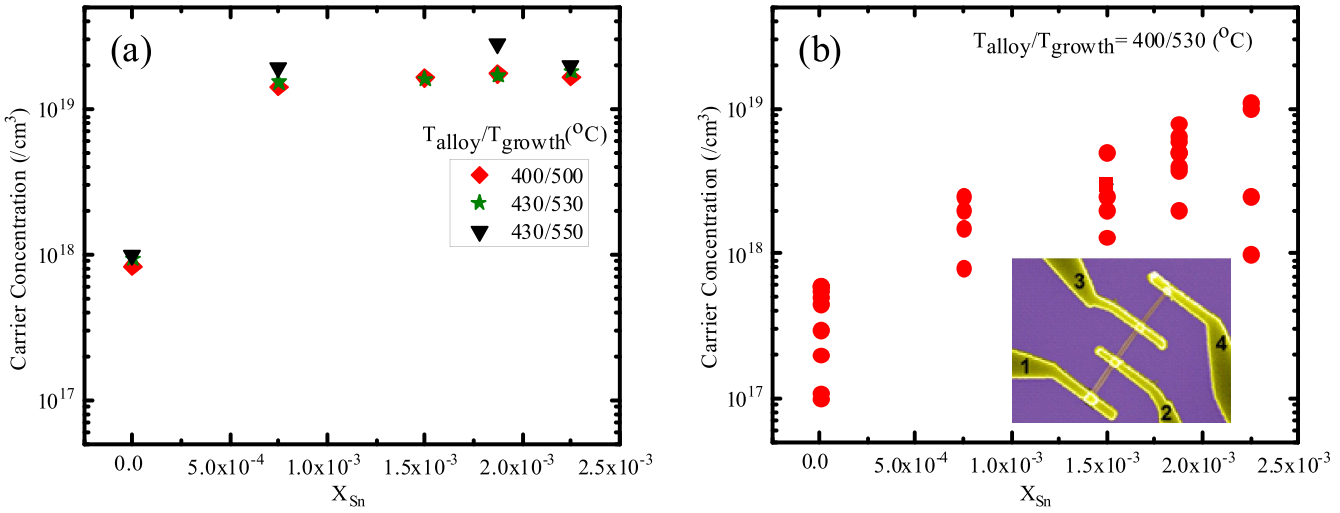

Figure 8. (a) Carrier concentration estimated from 7 K photoluminescence FWHM, for the undoped nanowires and Fermi-tail method for *n*-type doped GaAs nanowires grown at varying alloying and growth temperatures and varying X_{Sn}. (b) Carrier concentration estimated from four-point probe resistivity measurement of GaAs nanowires grown at alloying and growth temperature of 400 °C and 530 °C and with varying X_{Sn} (0.00–2.25 × 10^{-3}). Inset is the SEM image of a contacted nanowire.

is extracted by fitting to the tail of the PL spectrum, which provides information only about the highest doping in the sample cluster and is insensitive to variations within the cluster. Electrical measurements where single NWs are studied, reveal variations in carrier concentration within the same doping group. The spatial uniformity of dopant atoms in individual NWs was not studied thus far. Therefore, we assume bulk properties with uniform distribution, until further studies indicate otherwise.

4. Conclusions

n-type doping of pure zinc-blende GaAs nanowires with controlled morphology in Aerotaxy is reported for the first time with TESn as a precursor. This could serve as a road map in order to successfully dope III–V nanowires in Aerotaxy. The morphology of the doped nanowires was shown to be a strong function of both alloying and growth temperatures and of the dopant precursor flow.

Carrier concentration up to 10^{19} cm^{-3} could be estimated from our PL and confirmed by four-point probe resistivity measurements. The carrier concentration among samples varied slightly regardless of the change in alloying and growth temperature and dopant precursor flow. This insensitivity of the concentration with respect to different growth conditions helped to achieve good morphology wires without compromising the desired carrier concentration. However, in order to achieve lower carrier concentrations in a more controlled way, much lower flows of TESn should be considered. Furthermore, in order to reduce the carbon impurities in Aerotaxy wires, an alternative source of dopant such as H_2S could be a better alternative, this could also help to improve the morphology and growth rate of GaAs nanowires.

Acknowledgments

This work was performed in NanoLund at Lund University and within the MyFab cleanroom infrastructure; and with financial support from the Swedish Research Council (VR), the Swedish Energy Agency, the European Union's Horizon 2020 research and innovation programme under grant agreement No. 641023, and from the Knut and Alice Wallenberg Foundation (KAW). We acknowledge Jonas Johansson, Bengt Meuller and the Aerotaxy team at Sol Voltaics AB for their technical support and/or discussions.

Author contributions

The manuscript was written with contributions from all authors. All authors have given approval to the final version of the manuscript.

ORCID iDs

Wondwosen Metaferia https://orcid.org/0000-0003-1581-830X
Sudhakar Sivakumar https://orcid.org/0000-0002-0205-9036
Axel R Persson https://orcid.org/0000-0002-0399-8369
Irene Geijselaers https://orcid.org/0000-0001-9911-1672
L Reine Wallenberg https://orcid.org/0000-0002-0850-0398
Knut Deppert https://orcid.org/0000-0002-0471-951X
Lars Samuelson https://orcid.org/0000-0003-1971-9894
Martin H Magnusson https://orcid.org/0000-0002-8049-2142

References

[1] Berg A, Yazdi S, Nowzari A, Storm K, Jain V, Vainorius N, Samuelson L, Wagner J B and Borgström M T 2016 Radial nanowire light-emitting diodes in the $(Al_xGa_{1-x})_yIn_{1-y}P$ material system *Nano Lett.* **16** 656–62

[2] Chen X, Wong C K Y, Yuan C A and Zhang G 2013 Nanowire-based gas sensors *Sensors Actuators* B **177** 178–95

[3] Larrieu G and Han X-L 2013 Vertical nanowire array-based field effect transistors for ultimate scaling *Nanoscale* **5** 2437–41

[4] Åberg I *et al* 2016 A GaAs nanowire array solar cell with 15.3% efficiency at 1 sun *IEEE J. Photovolt.* **6** 185–90

[5] Wallentin J *et al* 2013 InP nanowire array solar cells achieving 13.8% efficiency by exceeding the ray optics limit *Science* **339** 1057–60

[6] Anttu N and Xu H Q 2013 Efficient light management in vertical nanowire arrays for photovoltaics *Opt. Express* **21** A558–75

[7] Fortuna S A, Wen J, Chun I S and Li X 2008 Planar GaAs nanowires on GaAs (100) substrates: self-aligned, nearly twin-defect free, and transfer-printable *Nano Lett.* **8** 4421–7

[8] Borgström M, Deppert K, Samuelson L and Seifert W 2004 Size- and shape-controlled GaAs nano-whiskers grown by MOVPE: a growth study *J. Cryst. Growth* **260** 18–22

[9] Isakov I, Panfilova M, Sourribes M J L, Tileli V, Porter A E and Warburton P A 2013 $InAs_{1-x}P_x$ nanowires grown by catalyst-free molecular-beam epitaxy *Nanotechnology* **24** 085707

[10] Mariager S O, Sørensen C B, Aagesen M, Nygård J, Feidenhans'l R and Willmott P R 2007 Facet structure of GaAs nanowires grown by molecular beam epitaxy *Appl. Phys. Lett.* **91** 083106

[11] Persson A I, Larsson M W, Stenström S, Ohlsson B J, Samuelson L and Wallenberg L R 2004 Solid-phase diffusion mechanism for GaAs nanowire growth *Nat. Mater.* **3** 677

[12] Núñez C G, Braña A F, López N and García B J 2015 On the growth mechanisms of GaAs nanowires by Ga-assisted chemical beam epitaxy *2015 10th Spanish Conf. on Electron Devices (CDE)* pp 1–4

[13] Heurlin M, Magnusson M H, Lindgren D, Ek M, Wallenberg L R, Deppert K and Samuelson L 2012 Continuous gas-phase synthesis of nanowires with tunable properties *Nature* **492** 90–4

[14] Metaferia W *et al* 2016 GaAsP nanowires grown by Aerotaxy *Nano Lett.* **16** 5701–7

[15] Arab S, Yao M, Zhou C, Dapkus P D and Cronin S B 2016 Doping concentration dependence of the photoluminescence spectra of n-type GaAs nanowires *Appl. Phys. Lett.* **108** 182106

[16] Yang F, Messing M E, Mergenthaler K, Ghasemi M, Johansson J, Wallenberg L R, Pistol M-E, Deppert K, Samuelson L and Magnusson M H 2015 Zn-doping of GaAs nanowires grown by Aerotaxy *J. Cryst. Growth* **414** 181–6

[17] Barrigón E, Hultin O, Lindgren D, Yadegari F, Magnusson M H, Samuelson L, Johansson L I M and Björk M T 2018 GaAs nanowire pn-junctions produced by low-cost and high-throughput Aerotaxy *Nano Lett.* **18** 1088–92

[18] Magnusson M H, Deppert K, Malm J-O, Bovin J-O and Samuelson L 1999 Gold nanoparticles: production, reshaping, and thermal charging *J. Nanopart. Res.* **1** 243–51

[19] Zhang S-H, Akutsu Y, Russell L M, Flagan R C and Seinfeld J H 1995 Radial differential mobility analyzer *Aerosol Sci. Technol.* **23** 357–72

[20] Ghasemi M and Johansson J 2017 Phase diagrams for understanding gold-seeded growth of GaAs and InAs nanowires *J. Phys. D: Appl. Phys.* **50** 134002

[21] Hultin O, Otnes G, Borgström M T, Björk M, Samuelson L and Storm K 2016 Comparing Hall effect and field effect measurements on the same single nanowire *Nano Lett.* **16** 205–11

[22] Chikyow T and Koguchi N 1990 MBE growth method for pyramid-shaped GaAs micro crystals on ZnSe(001) surface using Ga droplets *Japan. J. Appl. Phys.* **29** L2093

[23] Burgess T *et al* 2016 Doping-enhanced radiative efficiency enables lasing in unpassivated GaAs nanowires *Nat. Commun.* **7** 11927

[24] Kuech T F and Veuhoff E 1984 Mechanism of carbon incorporation in MOCVD GaAs *J. Cryst. Growth* **68** 148–56

[25] Joyce H J *et al* 2008 High purity GaAs nanowires free of planar defects: growth and characterization *Adv. Funct. Mater.* **18** 3794–800

[26] Lindgren D, Hultin O, Heurlin M, Storm K, Borgström M T, Samuelson L and Gustafsson A 2015 Study of carrier concentration in single InP nanowires by luminescence and Hall measurements *Nanotechnology* **26** 045705

[27] De-Sheng J, Makita Y, Ploog K and Queisser H J 1982 Electrical properties and photoluminescence of Te-doped GaAs grown by molecular beam epitaxy *J. Appl. Phys.* **53** 999–1006

[28] Sze S M and Irvin J C 1968 Resistivity, mobility and impurity levels in GaAs, Ge, and Si at 300 K *Solid-State Electron.* **11** 599–602